

Planar thermal Hall effect from phonons in a Kitaev candidate material

Lu Chen^{1*}, Étienne Lefrançois^{1*}, Ashvini Vallipuram¹, Quentin Barthélemy¹, Amirreza Ataei¹, Weiliang Yao², Yuan Li^{2,3}, and Louis Taillefer^{1,4}

1 Institut quantique, Département de physique & RQMP, Université de Sherbrooke, Sherbrooke, Québec, Canada

2 International Center for Quantum Materials, School of Physics, Peking University, Beijing, China

3 Collaborative Innovation Center of Quantum Matter, Beijing, China

4 Canadian Institute for Advanced Research, Toronto, Ontario, Canada

Kitaev materials are a promising platform for the realization of quantum spin liquid states. The thermal Hall effect has emerged as a potential probe of exotic excitations within such states. In the Kitaev candidate material α -RuCl₃, however, the thermal Hall conductivity κ_{xy} has been attributed not only to exotic Majorana fermions [1,2] or chiral magnons [3], but also to phonons [4]. It has been shown theoretically that the former two types of heat carriers can generate a “planar” thermal Hall effect [5-7], whereby the magnetic field is parallel to the heat current, as observed experimentally [3,8], but it is unknown whether phonons also could. Here we show that a planar thermal Hall effect is present in another Kitaev candidate material, Na₂Co₂TeO₆. On the basis of a striking similarity between the temperature and field dependence of κ_{xy} and that of the phonon-dominated thermal conductivity κ_{xx} , we argue that the planar thermal Hall effect in Na₂Co₂TeO₆ is generated

by phonons. The phonon contributed planar κ_{xy} also shows a strong sample dependence, which indicates an extrinsic origin of the mechanism. By conducting a complete study with different in-plane configurations of heat current J and magnetic field H , *i.e.* $H // J$ and $H \perp J$, we observe a large difference in κ_{xy} between these two configurations, which reveals that the direction of the heat current J may play an important role in determining the planar thermal Hall effect. Our observation calls for a re-evaluation of the planar thermal Hall effect observed in α -RuCl₃.

The quest for quantum spin liquids (QSLs) has attracted tremendous interest due to the potential realization of non-Abelian statistics and novel exotic excitations [9]. A promising platform for the realization of QSLs is the Kitaev model, which features bond-dependent Ising interactions between spin-1/2 degrees of freedom on a honeycomb lattice [10]. The Kitaev model is exactly solvable, and it predicts the existence of itinerant Majorana fermions that carry heat and should therefore contribute to thermal transport [5]. A topologically protected edge current can emerge from the bulk Majorana bands under an external magnetic field and be detected by the thermal Hall effect as a half-quantized thermal Hall conductivity κ_{xy} [11,12].

The search for Kitaev QSLs in real materials has focused on $5d$ iridium [13] and $4d$ ruthenium compounds [14], of which the quasi-2D Mott insulator α -RuCl₃ has been the most intensively studied. In α -RuCl₃, antiferromagnetic (AF) order sets in below a temperature $T_N \simeq 7$ K, with a spin configuration called “zigzag” order, but the application of a magnetic field H parallel to the honeycomb layers suppresses this order for $H \gtrsim 7$ T, thereby raising the possibility of a field-induced QSL state at low temperature when $H \gtrsim 7$ T. A half-quantized κ_{xy}

(*i.e.*, $\kappa_{xy}^{2D}/T = \pi k_B^2/6\hbar$) was reported in α -RuCl₃ – for an in-plane field in excess of 7 T – and interpreted as evidence of itinerant Majorana fermions [1,2]. The half-quantized κ_{xy} plateau appears even for a “planar” Hall configuration [8], *i.e.*, when the magnetic field is applied within the 2D plane and parallel to the heat current J , specifically for $H // a$, where a is the crystal direction perpendicular to the Ru-Ru bond (the so-called zigzag direction). Subsequently, Czajka *et al.* reported that the planar κ_{xy} in α -RuCl₃ shows no sign of half-quantization, and they instead attributed its smooth growth with temperature for $H // J // a$ to chiral magnons [3]. Theoretical work has shown that Majorana fermions [5] and topological magnons [6,7] are both able to generate a planar κ_{xy} in α -RuCl₃, when $H // a$.

In contrast to these two scenarios of exotic topological excitations, it has also been argued that phonons are the main carriers responsible for the thermal Hall effect in α -RuCl₃ – at least for a field normal to the 2D planes ($H // c$ and $J // a$) [4]. The argument is based on the striking similarity of $\kappa_{xy}(T)$ to $\kappa_{xx}(T)$, the phonon-dominated longitudinal thermal conductivity. However, it remains unknown whether phonons can also generate a planar κ_{xy} , where $H // J // a$.

Note that a non-zero planar Hall effect – *i.e.* a non-zero ΔT_y for $H // x$ in Fig. 1c and 1d – is in principle only allowed if the crystal structure of a material breaks three symmetries: the xy and yz planes are *not* mirror planes, and the C_2 rotational symmetry is broken along the x direction. In the monoclinic α -RuCl₃ (space group $C2/m$), the honeycomb (ab) plane is not a mirror plane, nor is the plane normal to the a axis. Furthermore, the C_2 rotational symmetry is broken along the a axis, so a planar κ_{xy} is allowed by symmetry for $H // a$, and is indeed observed [3,8]. However, the plane normal to the b direction *is* a mirror plane and the C_2

rotational symmetry is also preserved along the b direction; consistently, measurements report $\kappa_{xy} \simeq 0$ for $H \parallel b$ [8].

Here we turn to another Kitaev magnet candidate, the insulating material $\text{Na}_2\text{Co}_2\text{TeO}_6$ [15,16], and present a study of its planar thermal Hall effect. $\text{Na}_2\text{Co}_2\text{TeO}_6$ is a honeycomb-layered insulator (Fig. 1a) that develops long-range AF order below $T_N \simeq 27$ K [17] – which resembles the low-temperature formation of AF order in $\alpha\text{-RuCl}_3$. It has been theoretically predicted that the Kitaev model can also be realized in materials with d^7 ions such as Co^{2+} [18-20] and magnetic excitations in $\text{Na}_2\text{Co}_2\text{TeO}_6$ indeed resemble calculations based on extended Kitaev-Heisenberg models [21-26]. In our thermal transport study, the magnetic field H and heat current J are both applied in the ab plane, either parallel to each other (Fig. 1c) or perpendicular to each other (Fig. 1d). κ_{xx} and κ_{xy} are measured simultaneously, for four configurations: $H \parallel J \parallel a$ (perpendicular to the Co-Co bond direction), $H \parallel J \parallel a^*$ (parallel to the Co-Co bond direction), $J \parallel a$ & $H \parallel a^*$, and $J \parallel a^*$ & $H \parallel a$. Note that the structure of $\text{Na}_2\text{Co}_2\text{TeO}_6$ is such that a non-zero κ_{xy} is not allowed for either $H \parallel a$ or $H \parallel a^*$ because its crystal structure (space group $P6_322$) has C_2 rotational symmetry along both a and a^* directions.

First, we measured κ_{xx} and κ_{xy} in the two planar-parallel configurations, *i.e.* $H \parallel J \parallel a$ and $H \parallel J \parallel a^*$ (as shown in Fig 1c). In Fig. 2a, we show the thermal conductivity κ_{xx} of $\text{Na}_2\text{Co}_2\text{TeO}_6$ as a function of temperature, measured in sample A with configuration $H \parallel J \parallel a$, for $H = 0, 5, 10$ and 15 T. When $H \leq 10$ T, κ_{xx} shows little field dependence. Applying 15 T, however, produces a dramatic enhancement of κ_{xx} at low T , in agreement with prior data [27,28]. A similar behaviour is observed in $\alpha\text{-RuCl}_3$ [29,30], with a sudden increase of κ_{xx} when

$H > 7$ T. In both materials, κ_{xx} is attributed to phonons that are strongly scattered by spin fluctuations. When a field large enough to suppress AF order is applied in the 2D plane, a spin gap opens in the field-polarized state [31], and so the spin scattering is reduced at low T , leading to an increase in κ_{xx} [27,29,30].

In Fig. 2b, we show the thermal Hall conductivity of $\text{Na}_2\text{Co}_2\text{TeO}_6$, measured on the same sample (A) in the same configuration ($H // J // a$), plotted as κ_{xy} vs T . Surprisingly, we observe a non-zero κ_{xy} , which is supposed to be forbidden by the two-fold rotational symmetry along this direction. $\kappa_{xy}(T)$ mirrors the evolution of $\kappa_{xx}(T)$ at different fields. At $H = 5$ T and 10 T, $\kappa_{xy}(T)$ and $\kappa_{xx}(T)$ both show a broad hump around 40 K, while at $H = 15$ T, both display the same dramatic increase at low T , peaking at $T \sim 10$ K. This striking similarity between $\kappa_{xy}(T)$ and $\kappa_{xx}(T)$ is compelling evidence that κ_{xy} is carried predominantly by phonons in $\text{Na}_2\text{Co}_2\text{TeO}_6$. Evidence from other insulators has indeed shown that for phonons κ_{xy} and κ_{xx} both increase in tandem [32-35]. By contrast, if κ_{xy} were caused by Majorana fermions or magnons (or any other spin-based excitation), there would be no reason for it to mimic the phonon-dominated $\kappa_{xx}(T)$.

In Figs. 2c and 2d, we report the equivalent study for the planar-parallel configuration $H // J // a^*$, performed on a second sample (B). Again, we observe a non-zero κ_{xy} signal with $H // J // a^*$, which is also supposed to be forbidden by the two-fold rotational symmetry along this direction. This observation shows that the actual mechanism behind the planar thermal Hall effect in this material remains effective even though the pristine lattice has two-fold rotational symmetry in the a^* direction. We see again a dramatic increase of both κ_{xy} and κ_{xx} when a field

of 15 T is applied, reinforcing the close correlation between κ_{xy} and κ_{xx} seen in the first configuration. Interestingly, we find that in the second configuration ($H // a^*$) the parallel increase of κ_{xy} and κ_{xx} at low T even begins at 10 T, further confirming that κ_{xy} mimics κ_{xx} . We infer that the critical field for suppressing the AF order in $\text{Na}_2\text{Co}_2\text{TeO}_6$ is slightly less than 10 T for $H // a^*$ (and more than 10 T for $H // a$).

To check the reproducibility of our data, we performed the same measurements on another two samples (C and D) that were cut from the same mother sample. κ_{xx} and κ_{xy} measured on sample C with $H // J // a$ and on sample D with $H // J // a^*$ are plotted in Extended Data Fig. 2. Similar behavior of κ_{xx} and κ_{xy} are observed in samples C and D. However, the magnitude of κ_{xy} shows a clear sample dependence, especially when comparing samples B and D, which points to an extrinsic origin of the planar thermal Hall effect in $\text{Na}_2\text{Co}_2\text{TeO}_6$. This sample dependence may also explain the much smaller magnitude of κ_{xy} reported in a prior study by Takeda *et al.* [28].

Based on the close similarity we observe – for the two distinct field directions – between the temperature and field dependence of the planar κ_{xy} and that of the phonon-dominated κ_{xx} , we conclude that phonons are responsible for the planar thermal Hall conductivity κ_{xy} in $\text{Na}_2\text{Co}_2\text{TeO}_6$ – where field and current are both in the plane and parallel to each other. This shows it is possible – and makes it likely – that the planar κ_{xy} observed in $\alpha\text{-RuCl}_3$ is also carried by phonons.

In Fig. 3a, we compare the ratio of κ_{xy} over κ_{xx} , plotted as $\kappa_{xy} / \kappa_{xx}$ vs T , in all four samples. With a configuration of $H // J // a$, the ratio of sample C is about two times larger than

that of sample A, at $T = 20$ K. With a configuration of $H // J // a^*$, the ratio of sample B is about five times larger than that of sample D. Although a clear sample dependence is observed, the magnitude of $|\kappa_{xy} / \kappa_{xx}|$ in all cases is typical of the phonon thermal Hall effect found in various insulators (albeit for $H // z$) [33, 34, 35], where $0.05\% \lesssim \left| \frac{\kappa_{xy}}{\kappa_{xx}} \right| \lesssim 0.5\%$ at $T = 20$ K and $H = 15$ T. In Fig. 3b, we also see that the planar thermal Hall effect in $\text{Na}_2\text{Co}_2\text{TeO}_6$ is comparable – in both magnitude and temperature dependence – to that seen in $\alpha\text{-RuCl}_3$ for $H // J // a$ [36]. This striking similarity between $\text{Na}_2\text{Co}_2\text{TeO}_6$ and $\alpha\text{-RuCl}_3$ points to a common underlying mechanism.

After measuring both κ_{xx} and κ_{xy} with the heat current and magnetic field parallel to each other, we conduct the same measurements with H and J both in plane but perpendicular to each other ($H \perp J$). In Fig. 4a, we show the thermal conductivity κ_{xx} of $\text{Na}_2\text{Co}_2\text{TeO}_6$ at $H = 15$ T as a function of temperature with $H // a$, for two current directions: $J // H$ (sample C, $J // a$, red) and $J \perp H$ (sample D, $J // a^*$, blue). In Fig. 4c, we show the same comparison of current directions for $H // a^*$. We see that with the same field direction, κ_{xx} for $J \perp H$ is very similar in magnitude and temperature dependence to κ_{xx} for $J // H$. In other words, the current direction matters very little for κ_{xx} . However, as shown in Figs. 4b and 4d, κ_{xy} decreases dramatically when H changes from parallel to J to perpendicular to J . This observation clearly shows that the magnitude of the planar κ_{xy} strongly depends on the direction of the heat current relative to the magnetic field, *i.e.* whether $H // J$ or $H \perp J$. A similar behavior is also observed in sample A and sample B (Extended Data Fig. 3).

Three main questions arise. First, what makes phonons chiral in $\text{Na}_2\text{Co}_2\text{TeO}_6$? The sample dependence we observe suggests an extrinsic origin for the phonon thermal Hall effect, *e.g.* from scattering of phonons by defects or impurities. In a recent model, it was shown that defects embedded in an insulator with AF order can scatter phonons in a way that produces a thermal Hall effect in a magnetic field [37] – a mechanism that may well explain the dependence of κ_{xy} on impurity concentration in the AF insulator Sr_2IrO_4 [38].

The second question is: how can there be a non-zero κ_{xy} signal in $\text{Na}_2\text{Co}_2\text{TeO}_6$ when $H // J // a$ or $H // J // a^*$, two field directions for which a non-zero κ_{xy} is in principle forbidden by the C_2 rotational symmetry? Clearly, this planar Hall effect cannot originate from some intrinsic scenario controlled entirely by the underlying crystal symmetry, such as the scenario of Majorana fermions or topological magnons. Instead, we suggest that it may be due to a local symmetry breaking induced by some extrinsic effects. For example, by structural defects like stacking faults or domains, reminiscent of the proposal that structural domains play a role in generating a phonon thermal Hall effect in SrTiO_3 [32]. Indeed, it has been reported that the Na layers in $\text{Na}_2\text{Co}_2\text{TeO}_6$ are highly disordered [16], which could possibly break the local crystal symmetry.

The third question is: how to understand the large difference in the magnitude of κ_{xy} between $H // J$ and $H \perp J$? Our results indicate that when putting both H and J in the plane, the planar κ_{xy} can be dramatically reduced when current and field are perpendicular to each other. In previous theoretical explanations [6-8] for the planar thermal Hall effect observed in RuCl_3 , whether a non-zero planar κ_{xy} can arise only depends on the underlying crystal symmetry and

the direction of magnetic field, regardless of the direction of heat current. Our findings reveal that the direction of heat current also plays an important role in producing the planar thermal Hall effect. This calls for a re-evaluation of the mechanism responsible for the planar κ_{xy} observed in RuCl_3 .

Note that in addition to $\text{Na}_2\text{Co}_2\text{TeO}_6$, we have also observed a phononic planar thermal Hall signal (comparable in magnitude to the conventional thermal Hall signal) in both cuprates [39] and in the frustrated antiferromagnetic insulator Y-kapellasite [40], thereby further validating the existence of a planar thermal Hall signal coming from phonons.

References

- [1] Kasahara, Y. *et al.* Majorana quantization and half-integer thermal quantum Hall effect in a Kitaev spin liquid. *Nature* **559**, 227-231 (2018).
- [2] Bruin, J. A. N. *et al.* Robustness of the thermal Hall effect close to half-quantization in $\alpha\text{-RuCl}_3$. *Nat. Phys.* **18**, 401–405 (2022).
- [3] Czajka, P. *et al.* Planar thermal Hall effect of topological bosons in the Kitaev magnet $\alpha\text{-RuCl}_3$. *Nat. Mater.* **22**, 36–41 (2023).
- [4] Lefrançois, E. *et al.* Evidence of a phonon Hall effect in the Kitaev spin liquid candidate $\alpha\text{-RuCl}_3$. *Phys. Rev. X* **12**, 021025 (2022).
- [5] Nasu, J. *et al.* Thermal transport in the Kitaev model. *Phys. Rev. Lett.* **119**, 127204 (2017).
- [6] Li, E. C. *et al.* Sign structure of thermal Hall conductivity and topological magnons for in-plane field polarized Kitaev magnets. *Phys. Rev. Lett.* **126**, 147201 (2021).
- [7] Zhang, E. Z. *et al.* Topological magnons for thermal Hall transport in frustrated magnets with bond-dependent interactions. *Phys. Rev. B* **103**, 174402 (2021).
- [8] Yokoi, T. *et al.* Half-integer quantized anomalous thermal Hall effect in the Kitaev material candidate $\alpha\text{-RuCl}_3$. *Science* **373**, 568-572 (2021).

- [9] Savary, L. and Balents, L. Quantum spin liquids: a review. *Rep. Prog. Phys.* **80**, 016502 (2017).
- [10] Kitaev, A. Anyons in an exactly solved model and beyond. *Ann. Phys.* **321**, 2-111 (2006).
- [11] Ye, M. *et al.* Quantization of the thermal Hall conductivity at small Hall angles, *Phys. Rev. Lett.* **121**, 147201 (2018).
- [12] Vinkler-Aviv, Y. *et al.* Approximately quantized thermal Hall effect of chiral liquids coupled to phonons, *Phys. Rev. X* **8**, 031032 (2018).
- [13] Jackeli, G. and Khaliullin, G. Mott insulators in the strong spin-orbit coupling limit: from Heisenberg to a quantum compass and Kitaev models. *Phys. Rev. Lett.* **102**, 017205 (2009).
- [14] Banerjee, A. *et al.* Proximate Kitaev quantum spin liquid behaviour in a honeycomb magnet. *Nat. Mater.* **15**, 733-740 (2016).
- [15] Yao, W. L. and Li, Y. Ferrimagnetism and anisotropic phase tunability by magnetic fields in $\text{Na}_2\text{Co}_2\text{TeO}_6$. *Phys. Rev. B* **101**, 085120 (2020).
- [16] Viciu, L. *et al.* Structure and basic magnetic properties of the honeycomb lattice compounds $\text{Na}_2\text{Co}_2\text{TeO}_6$ and $\text{Na}_3\text{Co}_2\text{SbO}_6$. *J. Solid State Chem.* **180**, 1060 (2007).
- [17] Bera, A. K. *et al.* Zigzag antiferromagnetic ground state with anisotropic correlation lengths in the quasi-two-dimensional honeycomb lattice compound $\text{Na}_2\text{Co}_2\text{TeO}_6$. *Phys. Rev. B* **95**, 094424 (2017).
- [18] Liu, H. M. and Khaliullin, G. Pseudospin exchange interactions in d^7 cobalt compounds: Possible realization of the Kitaev model. *Phys. Rev. B* **97**, 014407 (2018).
- [19] Sano, R. *et al.* Kitaev-Heisenberg Hamiltonian for high-spin d^7 Mott insulators, *Phys. Rev. B* **97**, 014408 (2018).
- [20] Liu, H. M. *et al.* Kitaev spin liquid in $3d$ transition metal compounds. *Phys. Rev. Lett.* **125**, 047201 (2020).
- [21] Songvilay, M. *et al.* Kitaev interactions in the Co honeycomb antiferromagnets $\text{Na}_3\text{Co}_2\text{SbO}_6$ and $\text{Na}_2\text{Co}_2\text{TeO}_6$. *Phys. Rev. B* **102**, 224429 (2020).

- [22] Lin, G. *et al.* Field-induced quantum spin disordered state in spin-1/2 honeycomb magnet $\text{Na}_2\text{Co}_2\text{TeO}_6$. *Nat. Commun.* **12**, 5559 (2021).
- [23] Chen, W. J. *et al.* Spin-orbit phase behaviors of $\text{Na}_2\text{Co}_2\text{TeO}_6$ at low temperatures. *Phys. Rev. B* **103**, L180404 (2021).
- [24] Kim, C. *et al.* Antiferromagnetic Kitaev interaction in $J_{\text{eff}} = 1/2$ cobalt honeycomb materials $\text{Na}_3\text{Co}_2\text{SbO}_6$ and $\text{Na}_2\text{Co}_2\text{TeO}_6$. *J. Phys.: Condens. Matter* **34**, 045802 (2022).
- [25] Samarakoon, A. M. *et al.* Static and dynamic magnetic properties of honeycomb lattice antiferromagnets $\text{Na}_2\text{M}_2\text{TeO}_6$, $\text{M} = \text{Co}$ and Ni . *Phys. Rev. B* **104**, 184415 (2021).
- [26] Yao, Weiliang *et al.* Excitations in the ordered and paramagnetic states of honeycomb magnet $\text{Na}_2\text{Co}_2\text{TeO}_6$. *Phys. Rev. Lett.* **129**, 147202 (2022).
- [27] Hong, X. *et al.* Strongly scattered phonon heat transport of the candidate Kitaev material $\text{Na}_2\text{Co}_2\text{TeO}_6$. *Phys. Rev. B* **104**, 144426 (2021).
- [28] Takeda, H. *et al.* Planar thermal Hall effects in Kitaev spin liquid candidate $\text{Na}_2\text{Co}_2\text{TeO}_6$. *Phys. Rev. Res.* **4**, L042035 (2022).
- [29] Hentrich, R. *et al.* Unusual phonon heat transport in $\alpha\text{-RuCl}_3$: strong spin-phonon scattering and field-induced spin gap. *Phys. Rev. Lett.* **120**, 117204 (2018).
- [30] Hentrich, R. *et al.* High-field thermal transport properties of Kitaev quantum magnet $\alpha\text{-RuCl}_3$: Evidence for low-energy excitations beyond the critical field. *Phys. Rev. B* **102**, 235155 (2020).
- [31] Balz, C. *et al.* Finite field regime for a quantum spin liquid in $\alpha\text{-RuCl}_3$. *Phys. Rev. B* **100**, 060405(R) (2019).
- [32] Li, X. *et al.* Phonon thermal Hall effect in strontium titanate. *Phys. Rev. Lett.* **128**, 105901 (2020).
- [33] Boulanger, M.-E. *et al.* Thermal Hall conductivity in the cuprate Mott insulators Nd_2CuO_4 and $\text{Sr}_2\text{CuO}_2\text{Cl}_2$. *Nat. Commun.* **11**, 5325 (2020).
- [34] Chen, L. *et al.* Large phonon thermal Hall conductivity in a simple antiferromagnetic insulator. *PNAS* **119** e2208016119 (2022).

- [35] Li, X. *et al.* The phonon thermal Hall angle in black phosphorus. *Nat. Commun.* **14**, 1027 (2023).
- [36] Czajka, P. Exotic thermal transport in a Kitaev magnet. PhD thesis, Princeton (2022).
- [37] Guo, H., Joshi, D.-G. & Sachdev, S. Resonant thermal Hall effect of phonons coupled to dynamical defects. *PNAS* **119**, e2215141119 (2022).
- [38] Ataei, A. *et al.* Impurity-induced phonon thermal Hall effect in the antiferromagnetic phase of Sr_2IrO_4 . *Nat. Phys.* (in press); arXiv:2302.03796.
- [39] Chen, L. *et al.* Planar thermal Hall effect from phonons in cuprates. arXiv:2309.17231.
- [40] Barthélemy, Q. *et al.* Planar parallel phonon Hall effect and local symmetry breaking. arXiv:2310.19682.
- [41] Grissonnanche, G. *et al.* Giant thermal Hall conductivity in the pseudogap phase of cuprate superconductors. *Nature* **571**, 376-380 (2019).
- [42] Grissonnanche, G. *et al.* Chiral phonons in the pseudogap phase of cuprates. *Nat. Phys.* **16**, 1108-1111 (2020).

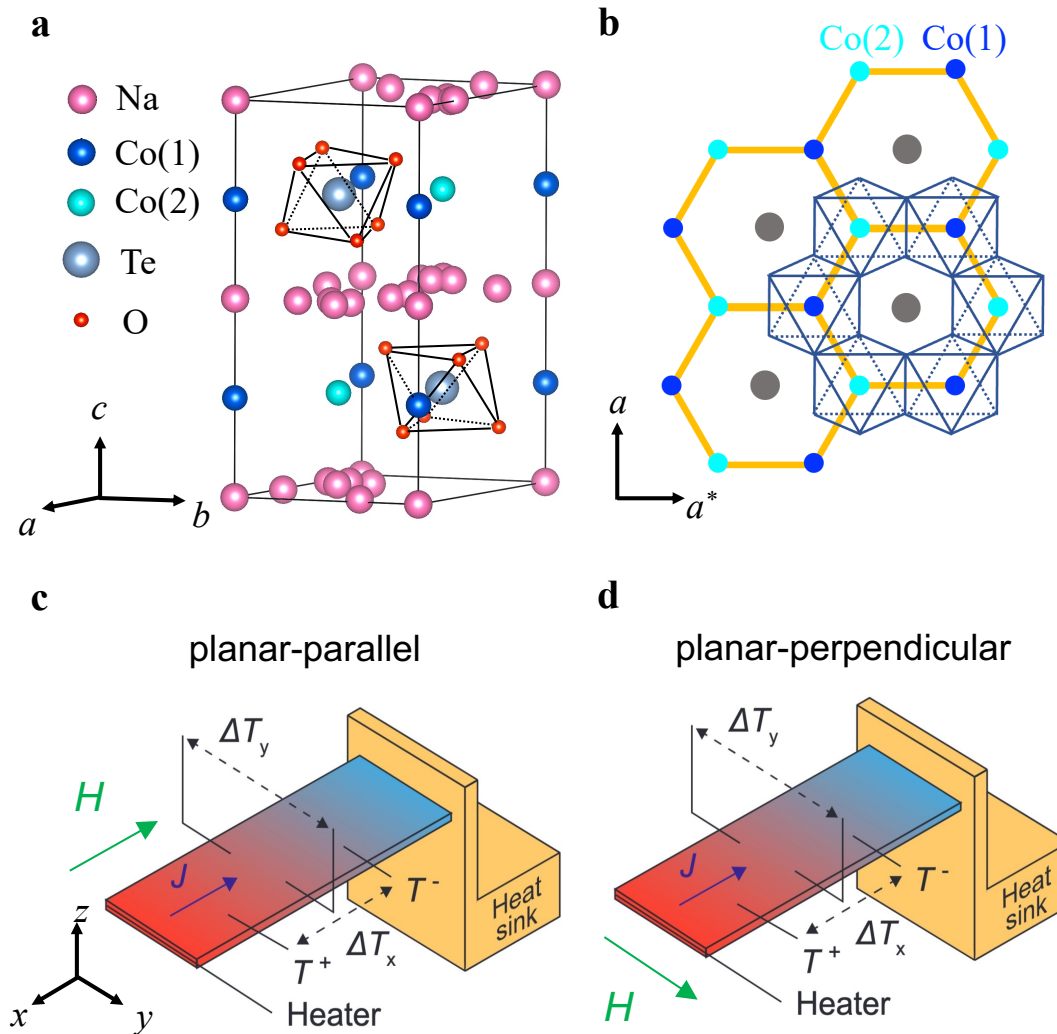


Fig. 1 | Crystal structure of $\text{Na}_2\text{Co}_2\text{TeO}_6$ and experimental setup.

a) The crystal structure of $\text{Na}_2\text{Co}_2\text{TeO}_6$. Honeycomb layers of edge-sharing CoO_6 octahedra sandwiched between Na layers and stacked along the c direction in an $ABAB$ format. The two types of inequivalent environments result in two different Co^{+2} sites which are labeled as Co (1) and Co (2). **b)** The honeycomb layer viewed along the crystal c axis. The Co^{+2} atoms are surrounded by oxygen octahedra. a denotes the zigzag direction (perpendicular to the Co-Co bond), a^* denotes the armchair direction (parallel to the Co-Co bond). Schematic of the thermal transport measurement setup with **c)** $H \parallel J$ and **d)** $H \perp J$ (see Methods). Directions of both thermal current J and external magnetic field H are shown with colored arrows.

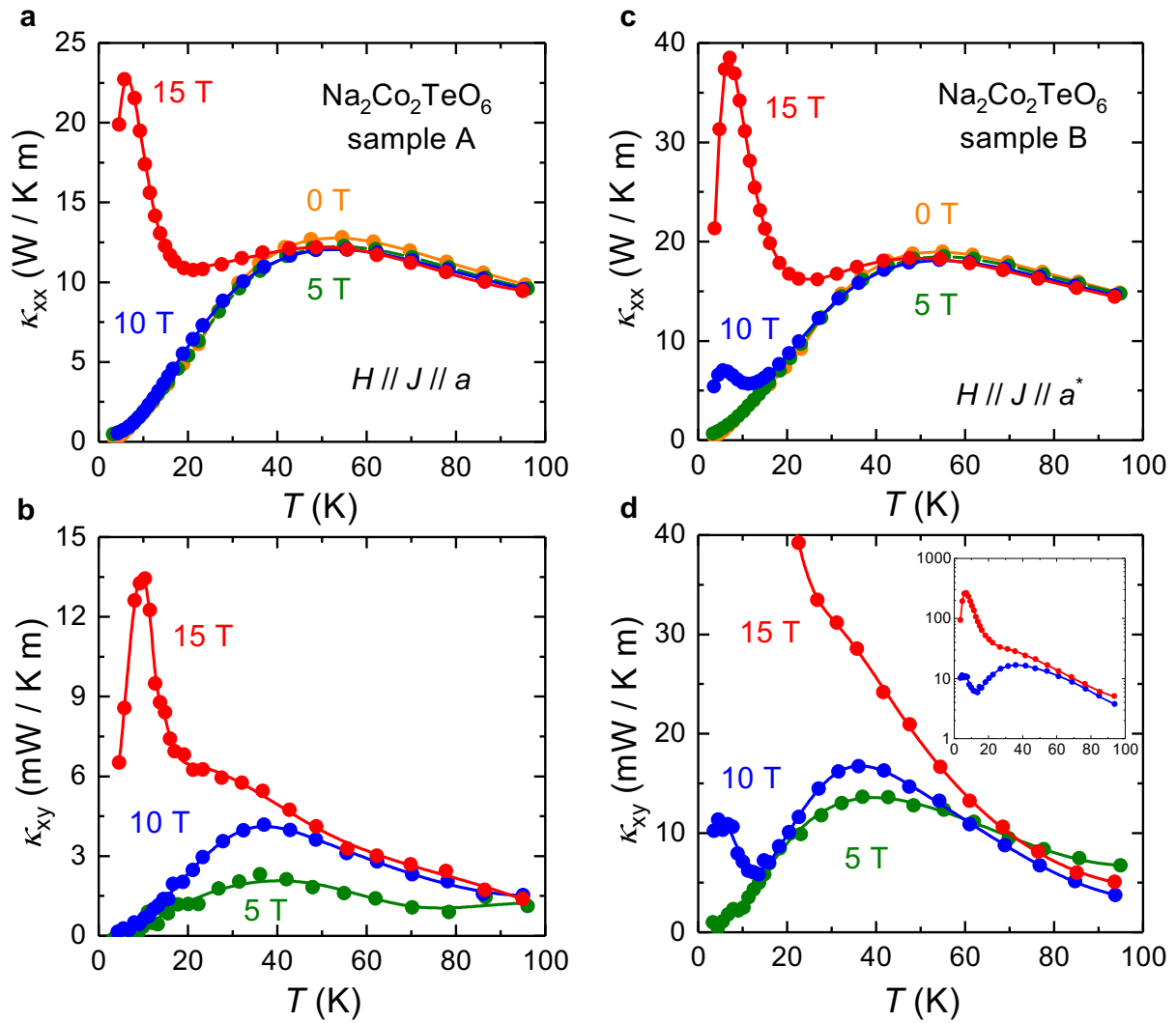


Fig. 2 | Thermal transport in $\text{Na}_2\text{Co}_2\text{TeO}_6$ with $H // J // a$ and $H // J // a^*$.

Thermal conductivity κ_{xx} vs T in $\text{Na}_2\text{Co}_2\text{TeO}_6$ **a)** sample A measured with $H // J // a$ and **c)** sample B measured with $H // J // a^*$ at $H = 0$ T, 5 T, 10 T, and 15 T. Thermal Hall conductivity κ_{xy} vs T in $\text{Na}_2\text{Co}_2\text{TeO}_6$ **b)** sample A and **d)** sample B measured at $H = 5$ T, 10 T, and 15 T. In panel **d)**, the inset shows the full range of data.

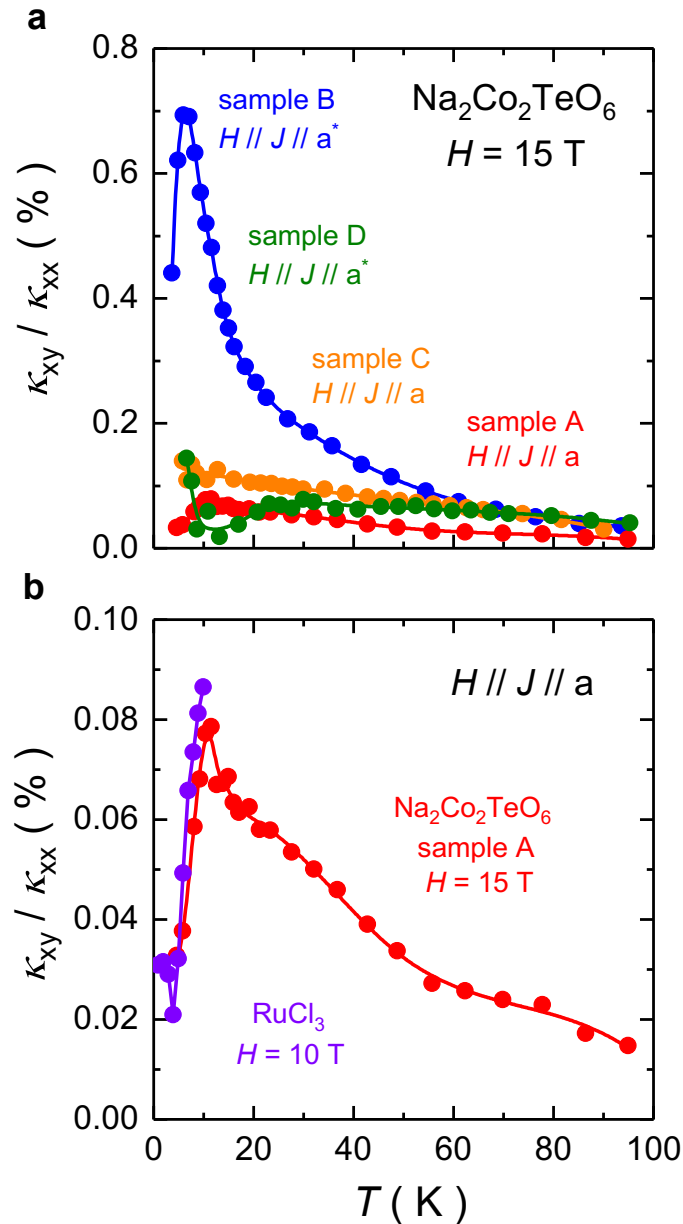


Fig. 3 | Ratio of $\kappa_{xy} / \kappa_{xx}$ for candidate Kitaev magnets.

a) Ratio $\kappa_{xy} / \kappa_{xx}$ vs T of the planar thermal Hall response in $\text{Na}_2\text{Co}_2\text{TeO}_6$ at $H = 15$ T of the four measured samples. Although the ratio clearly shows a sample dependence, the order of magnitude (0.1% at $H = 15$ T and $T = 20$ K) is typical of the phonon thermal Hall effect in various insulators [33,34,35]. **b)** Ratio $\kappa_{xy} / \kappa_{xx}$ vs T of the planar thermal Hall response in candidate Kitaev magnets $\text{Na}_2\text{Co}_2\text{TeO}_6$ and α - RuCl_3 . The purple curve is obtained from data in Fig 3.28 of Ref. [36].

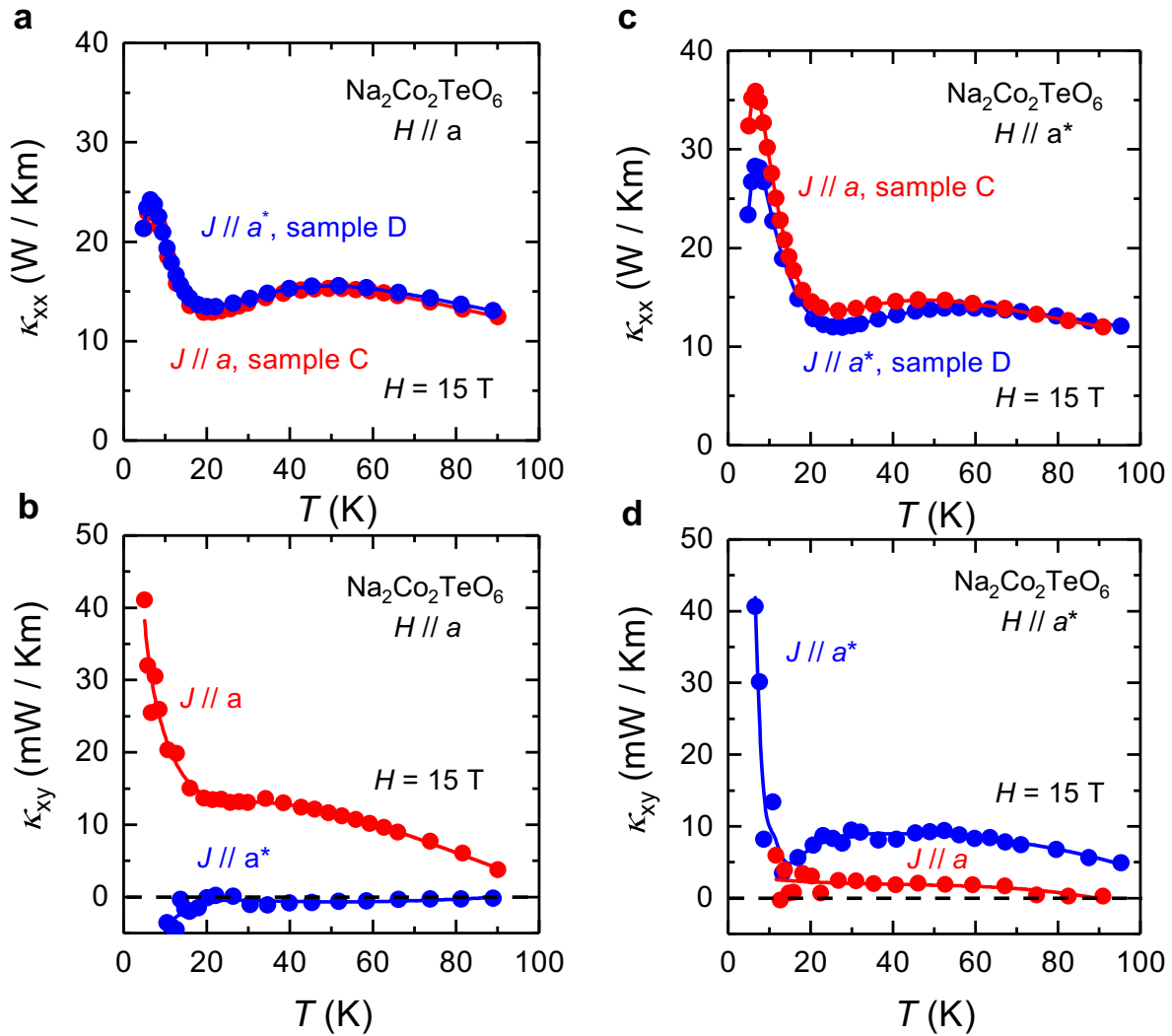


Fig. 4 | Thermal transport data in $\text{Na}_2\text{Co}_2\text{TeO}_6$ for $H // J$ and $H \perp J$.

a) Thermal conductivity κ_{xx} and **b)** thermal Hall conductivity κ_{xy} vs T in $\text{Na}_2\text{Co}_2\text{TeO}_6$ s, measured at $H = 15$ T for $H // a$: on sample C with $J // a$ (red) and sample D with $J // a^*$ (blue). **c, d)** Corresponding data for $H // a^*$. In both field directions, κ_{xy} measured with $H \perp J$ is much smaller than that measured with $H // J$.

Acknowledgements

L.T. acknowledges support from the Canadian Institute for Advanced Research (CIFAR) as a Fellow and funding from the Natural Sciences and Engineering Research Council of Canada (NSERC; PIN: 123817), the Fonds de recherche du Québec - Nature et Technologies (FRQNT), the Canada Foundation for Innovation (CFI), and a Canada Research Chair. This research was undertaken thanks in part to funding from the Canada First Research Excellence Fund. The work at Peking University was supported by the National Basic Research Program of China (Grant No. 2021YFA1401901) and the NSF of China (Grant No. 12061131004).

Author Information

The authors declare no competing financial interest. Correspondence and request for materials should be addressed to L.C. (lu.chen@usherbrooke.ca) or L.T. (louis.taillefer@usherbrooke.ca).

Data availability

The experimental data in the paper is available from the corresponding authors upon a reasonable request.

Author Contributions

*L.C. and É. L. contributed equally to this work.

W.Y. and Y.L. grew the $\text{Na}_2\text{Co}_2\text{TeO}_6$ single crystals. L.C. and A.V. prepared the samples. L.C., É.L., A.V., A.A. and Q.B. performed the thermal transport measurements. L.C. and L.T. wrote the manuscript, in consultation with all the authors. L.T. supervised the project.

METHODS

SAMPLES. Single crystals of $\text{Na}_2\text{Co}_2\text{TeO}_6$ were grown by a self-flux method starting from Na_2CO_3 , Co_3O_4 and TeO_2 in a molar ratio of 15.4 : 5.2 : 21.4. These oxides were ground thoroughly and put into an alumina crucible, which was then heated to 1323 K in 4 hours and maintained for 48 hours before being cooled down to 873 K in 6.5 K/hour. The furnace was turned off at 873 K to cool down to room temperature. Thin single crystals of hexagonal shape were harvested from the solidified flux. The edge of the hexagon is along the a axis of the crystal structure.

Four single crystal samples of $\text{Na}_2\text{Co}_2\text{TeO}_6$ were used in the heat transport measurements. Sample A has dimensions $L = 0.95$ mm (length between contacts, along x), $w = 1.62$ mm (width, along y) and $t = 0.1$ mm (thickness, along z), with the x direction (Fig. 1c) along the a axis of the crystal structure (Fig. 1b). Sample B has dimensions $L = 1.55$ mm (along x), $w = 2.83$ mm (along y) and $t = 0.07$ mm (along z), with the x direction along the a^* axis of the crystal structure (Fig. 1b). Sample C has dimensions $L = 0.84$ mm (length between contacts, along x), $w = 1.00$ mm (width, along y) and $t = 0.04$ mm (thickness, along z), with the x direction (Fig. 1c) along the a axis of the crystal structure (Fig. 1b). Sample D has dimensions $L = 1.43$ mm (along x), $w = 0.73$ mm (along y) and $t = 0.05$ mm (along z), with the x direction along the a^* axis of the crystal structure (Fig. 1b). Sample A and B are two separate as-grown samples, while sample C and sample D are cut from one as-grown mother sample that is from the same batch of A and B.

Contacts were made by attaching $50 \mu\text{m}$ diameter silver wires to the sample using silver paint. The heater was connected to the sample by $100 \mu\text{m}$ diameter silver wire by silver paint.

THERMAL TRANSPORT MEASUREMENTS. The thermal conductivity κ_{xx} and thermal Hall conductivity κ_{xy} were measured by applying a heat current J along the length of the sample ($J // x$; Fig. 1c and 1d) and a magnetic field H parallel to J ($H // x$; Fig. 1c) or perpendicular to J ($H // y$; Fig. 1d), in the so-called “planar” configuration. The current produces a longitudinal temperature difference ΔT_x along x (between the two contacts separated by the distance L). The thermal conductivity is defined as $\kappa_{xx} = (J / \Delta T_x)(L / wt)$. The field produces a transverse temperature difference ΔT_y along y (between the two sides of the sample, separated by the

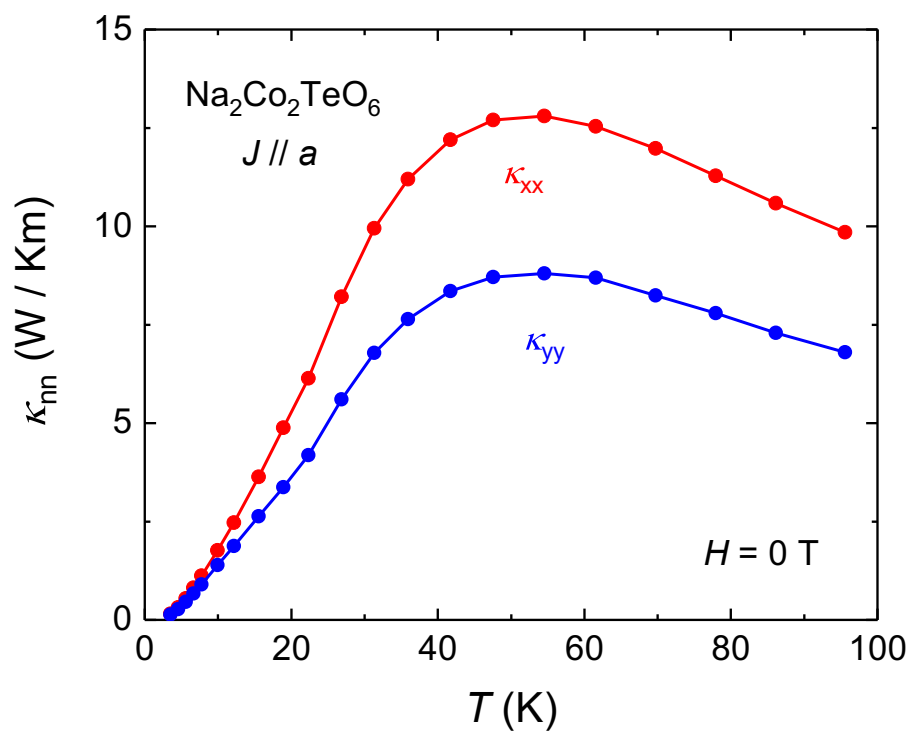
sample width w). The thermal Hall conductivity is defined as $\kappa_{xy} = -\kappa_{yy}(\Delta T_y / \Delta T_x)(L/w)$.

For sample A, the current and field directions are $J // H // a$ or $J // a \ \& \ H // a^*$, where a is perpendicular to the Co-Co bond direction in the lattice and a^* is parallel to the Co-Co bond direction. For sample B, $J // H // a^*$ or $J // a^* \ \& \ H // a$. In a honeycomb lattice, $\kappa_{xx} \neq \kappa_{yy}$. For sample A and B, we obtain κ_{yy} by multiplying the κ_{xx} measured on the same sample by the anisotropy factor κ_{yy}/κ_{xx} reported in Ref. [27] (see Extended Data Fig. 1). κ_{yy} and κ_{xx} reported in Ref. [27] are measured on two samples that are cut from the same mother sample, which reflects the intrinsic anisotropy of the longitudinal thermal conductivity when the heat current is applied along a or a^* direction. This anisotropy is also consistent with what we get from sample C and sample D, which are cut from the same mother samples.

The experimental technique used here was the same as described in Refs. [39, 40]. The heat current is generated by a resistive heater connected to one end of the sample (Fig. 1c and 1d). The other end of the sample is glued to a copper block with silver paint that acts as a heat sink. The longitudinal and transverse temperature differences ΔT_x and ΔT_y are measured using type-E thermocouples. All the measurements are conducted with a steady-state method in a variable temperature insert (VTI) system up to $H = 15$ T. The data was taken by changing temperature in discrete steps at a fixed magnetic field. After the temperature is stabilized at each temperature, the background value of the thermocouple is eliminated by subtracting the heater-off value from the heater-on value. When measuring κ_{xy} , the contamination from κ_{xx} due to a slight misalignment of contacts for ΔT_y is removed by doing field anti-symmetrization to the transverse temperature difference. That is to say, we measure ΔT_y with both positive and negative magnetic fields exactly in the same conditions, then the transverse temperature difference used to obtain κ_{xy} is defined as $\Delta T_y(H) = [\Delta T_y(T, +H) - \Delta T_y(T, -H)]/2$.

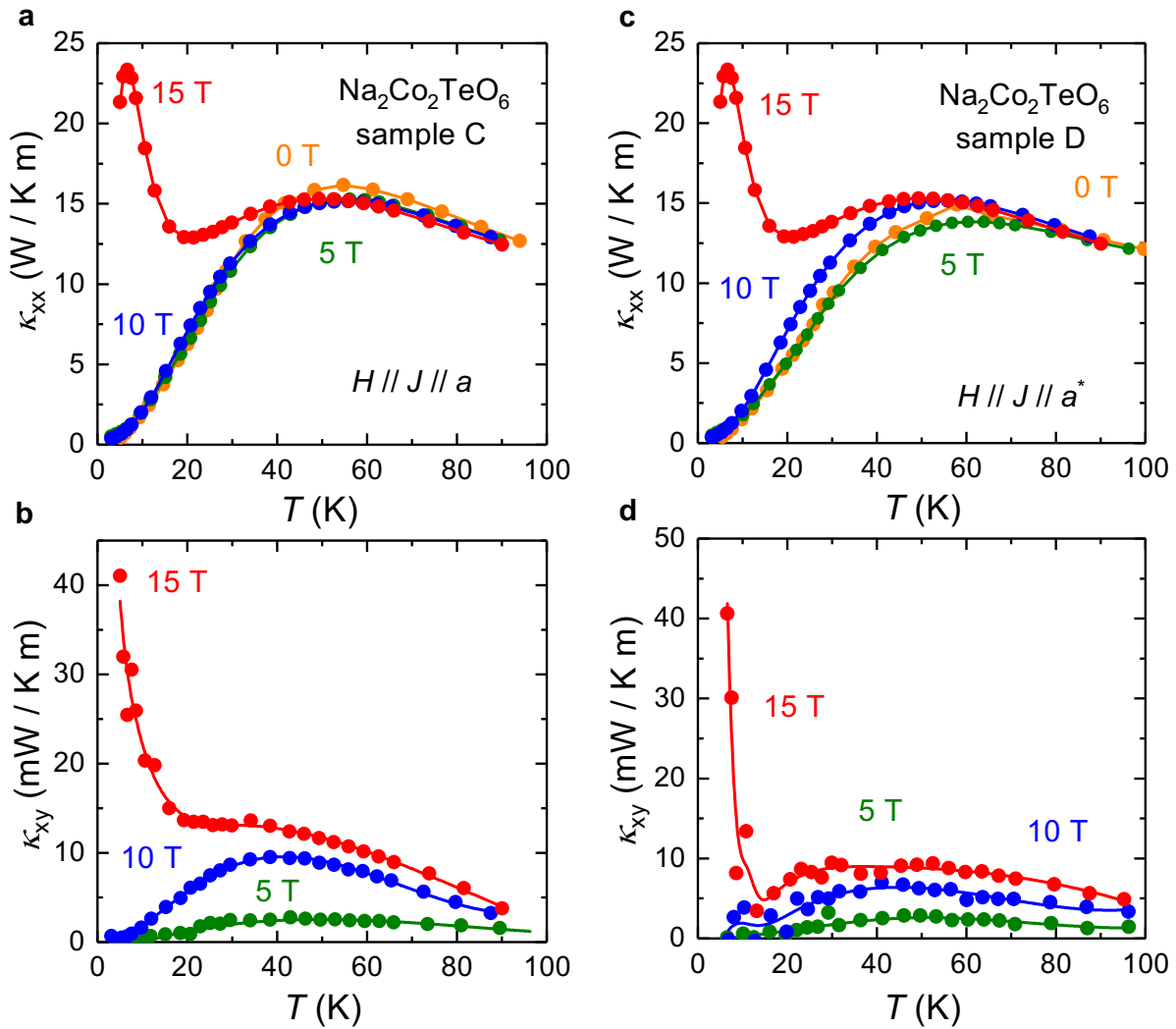
THERMAL CONDUCTIVITY AND THERMAL HALL CONDUCTIVITY MEASURED IN FOUR $\text{Na}_2\text{Co}_2\text{TeO}_6$ SAMPLES. κ_{xx} and κ_{xy} measured in sample C with $H // J // a$ and sample D with $H // J // a^*$ are plotted in Extended Data Fig. 2.

κ_{xx} and κ_{xy} measured in sample A with $H // J // a$ or $J // a \ \& \ H // a^*$ and sample B with $H // J // a^*$ or $J // a^* \ \& \ H // a$ are plotted in Extended Data Fig. 3.



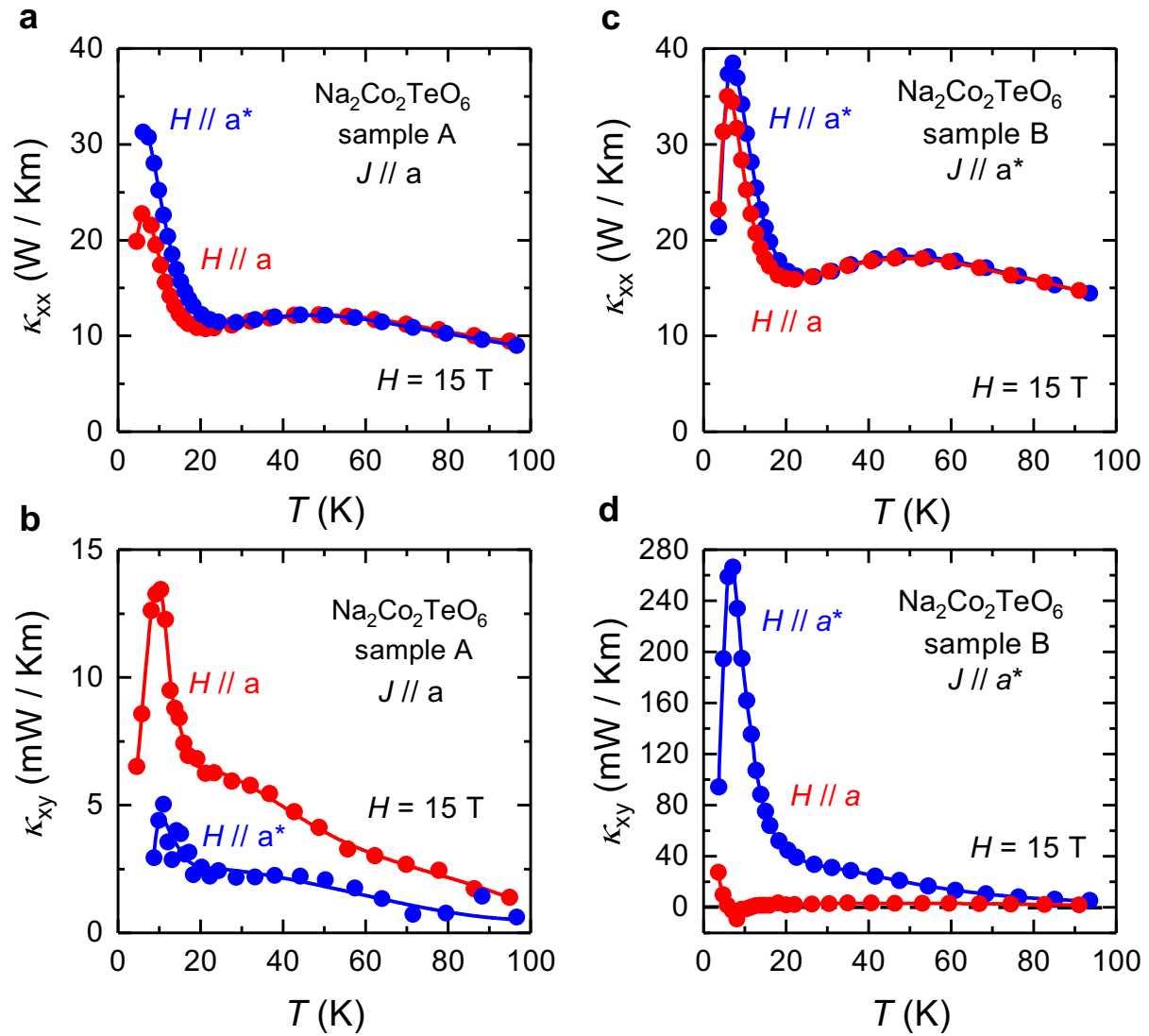
Extended Data Fig. 1 | Thermal conductivity data in $\text{Na}_2\text{Co}_2\text{TeO}_6$ with $J // a$.

Red curve is the thermal conductivity κ_{xx} vs T in $\text{Na}_2\text{Co}_2\text{TeO}_6$ sample A measured at $H = 0 \text{ T}$ with $J // a$. The thermal conductivity κ_{yy} at $H = 0 \text{ T}$ with $J // a^*$ in that sample (blue curve) is estimated by multiplying the κ_{xx} data by the anisotropy factor κ_{yy}/κ_{xx} reported in Ref. [27].



Extended Data Fig. 2 | Thermal transport in samples C and D.

Thermal conductivity κ_{xx} vs T in $\text{Na}_2\text{Co}_2\text{TeO}_6$, measured on sample C (a), measured with $H \parallel J \parallel a$, and sample D (c), measured with $H \parallel J \parallel a^*$, at $H = 0, 5, 10$ and 15 T. Corresponding thermal Hall conductivity κ_{xy} for sample C (b) and sample D (d).



Extended Data Fig. 3 | Comparing $H // J$ and $H \perp J$ in samples A and B.

a) Thermal conductivity κ_{xx} vs T and **b)** thermal Hall conductivity κ_{xy} vs T in $\text{Na}_2\text{Co}_2\text{TeO}_6$ measured on sample A with $J // a$ for $H // a$ (red) and $H // a^*$ (blue), at $H = 15$ T. **c, d)** Corresponding data for sample B, measured with $J // a^*$. We observe that κ_{xy} measured in the configuration $H \perp J$ is much smaller than in the configuration $H // J$.